doi.org/10.52568/001875/JCSP/48.02.2026

CO_2 Reduction Reaction to Create CH_4 and CH_3OH on Chromium Doped Silicon, Carbon and Boron Nitride (2Cr-Si_{76}, 2Cr-C_{76} and 2Cr-$B_{38}N_{38}$)

[1]Huaying Gao, [2]Xinxin Li*, [3]Chun Xiang
[1]*Library and Information Center of Weifang Engineering Vocational College, Weifang, Shandong, 262500, China.*
[2]*College of A&F Science and Technology, Weifang Engineering Vocational College, Weifang, Shandong, 262500, China.*
[3]*Shaoxing Hanli Industrial Automation, Shaoxing, Zhejiang, China.*
19228641905@163.com*

(Received on 30th April 2025, accepted in revised form 24th December 2025)

Abstract: Here, the pathways for CO_2 reduction reaction to create CH_4 and CH_3OH on Si_{76}, C_{76} and $B_{38}N_{38}$ as catalysts are investigated. The effects of adsorption of Cr on capacities of Si_{76}, C_{76} and $B_{38}N_{38}$ for CO_2-RR are examined. Results shown that the over-potential of CO_2-RR on 2Cr-Si_{76}, 2Cr-C_{76} and 2Cr-$B_{38}N_{38}$ are lower than Fe, Ni and Co single atom as catalysts, Cu, Au, Ag based bimetallic catalysts and Pt and Pd as metal catalysts in previous works. The $\Delta G_{reaction}$ of possible reaction steps of CO_2 reduction on 2Cr-Si_{76} and 2Cr-$B_{38}N_{38}$ nanocages are more negative than 2Cr-C_{76} nanocage. The over-potential for production of CH_4 and CH_3OH are lower than creation of HCOOH and HCHO on 2Cr-Si_{76}, 2Cr-C_{76} and 2Cr-$B_{38}N_{38}$ nanocages. The over-potential for CO, HCOOH, HCHO, CH_3OH and CH_4 production on 2Cr-$B_{38}N_{38}$ nanocage is 0.34, 0.27, 0.31, 0.24 and 0.22 V. The 2Cr-Si_{76} and 2Cr-$B_{38}N_{38}$ are catalyzed the reaction steps of CO_2-RR by three pathways and high performance.

Keyword: Nano-catalysts, CH_3OH, CO_2-RR, CH_4, reduction reaction mechanism, Metal adsorption.

Introduction

The carbon dioxide (CO_2) has been produced from fossil fuels [1] and CO_2 are one of the main reasons for earth warming [2]. The decreasing and removing the CO_2 has high important to reduce the earth warming [3-5]. The CO_2 can be removed in important reactions and CO_2 can be converted to other species with high performances [5-8]. The organic chemists have confirmed that the reduction reaction of CO_2 can create the HCOOH and CH_3OH molecules [9-11].

The Si and C nanocages and nanotubes have been proposed the novel pathways to design of stable and active catalysts for important reaction in chemical industry [12-14]. The capacities of metals doped Si and C nanocages and nanotubes to catalyze the important organic reactions in chemical industry have been examined [15-17]. Researchers shown than the Si, BN and C nanocages and nanotubes have effective properties for CO_2-RR in normal temperature [17]. In recent years, researchers have shown that the metal catalysts due to their high price, low stability, low selectivity and low performances have low efficiency for oxidation and reduction of toxic gases [11-15].

In previous works [11-15] the capacities of various metal catalysts including the Fe, Ni and Co single atom, Cu, Au, Ag based bimetallic and Pt and Pd as catalysts for CO_2-RR have been examined. The possible pathways for CO_2-RR on various metal catalysts including the Fe, Ni and Co single atom, Cu, Au, Ag based bimetallic and Pt and Pd have been investigated [11-15]. Results have shown that the metal catalysts (Fe, Ni and Co single atom, Cu, Au, Ag based bimetallic and Pt and Pd) have high price and low selectivity for catalyze the reaction steps of CO_2-RR in normal temperature [11-15].

In this work, the pathways for CO_2-RR for formation the CO, CH_4, HCOOH, HCHO and CH_3OH species on 2Cr-Si_{76}, 2Cr-C_{76} and 2Cr-$B_{38}N_{38}$ are investigated. The effects of adsorption of Cr atoms of 2Cr-Si_{76}, 2Cr-C_{76} and 2Cr-$B_{38}N_{38}$ on their capacities for CO_2-RR are examined. The capacities of 2Cr-Si_{76}, 2Cr-C_{76} and 2Cr-$B_{38}N_{38}$ for CO_2-RR are compared. The catalysts and pathways on 2Cr-Si_{76}, 2Cr-C_{76} and 2Cr-$B_{38}N_{38}$ for CO_2-RR are proposed with high efficiency. The goals of this work are: to compare the abilities of 2Cr-Si_{76}, 2Cr-C_{76} and 2Cr-$B_{38}N_{38}$ of CO_2-RR; to suggest the new catalysts (2Cr-Si_{76}, 2Cr-C_{76} and 2Cr-$B_{38}N_{38}$) for CO_2-RR, to compare the catalytic activity of various nanocages for CO_2-RR, to find the effective pathways for CO_2-RR, to compare the efficiency of 2Cr-Si_{76}, 2Cr-C_{76} and 2Cr-$B_{38}N_{38}$ for CO_2-RR with metal based catalysts.

*To whom all correspondence should be addressed.

Computational Details

The M06-2X/6-311+G (2d, 2p), PBEPBE/6-311+G (2d, 2p) and B3LYP-D3/6-311+G (2d, 2p) methods have been used to optimize the Si_{76}, C_{76}, $B_{38}N_{38}$, 2Cr-Si_{76}, 2Cr-C_{76} and 2Cr-$B_{38}N_{38}$ nanocages and their complexes with species in GAMESS software [16]. In this study the transition states of reaction step of CO_2-RR on 2Cr-Si_{76}, 2Cr-C_{76} and 2Cr-$B_{38}N_{38}$ have been obtained with opt=qst3 and results have shown that there is only one imaginary frequency for transition states of reaction step of CO_2-RR on 2Cr-Si_{76}, 2Cr-C_{76} and 2Cr-$B_{38}N_{38}$ [17-19]. In this study the COSMO (Conductor-like screening model) model as an implicit solvation model has been used to consider the effects of solvent (water as polar solvent) on reaction steps of possible mechanisms of CO_2-RR by M06-2X /6-311+G (2d, 2p) method [20].

In this study, the acceptable spin states and spin multiplicities (S = 3, 2 and 1 and 2S+1 = 7, 5 and 3) of Cr atoms in 2Cr-Si_{76}, 2Cr-C_{76} and 2Cr-$B_{38}N_{38}$ and complexes of 2Cr-Si_{76}, 2Cr-C_{76} and 2Cr-$B_{38}N_{38}$ with intermediates of CO_2-RR have been considered [19, 20]. The complexes of intermediates of CO_2-RR have been optimized and their frequencies have been calculated [20]. The adsorption free Gibbs energies ($\Delta G_{adsorption}$) of CO_2 and intermediates of CO_2-RR on 2Cr-Si_{76}, 2Cr-C_{76} and 2Cr-$B_{38}N_{38}$ are calculated [21]:

$$\Delta G_{adsorption} = G_{specie\text{-}nanocage} - G_{specie} - G_{nanocage} \quad (1)$$

The $G_{nanocage}$ is free Gibbs energies of 2Cr-Si_{76}, 2Cr-C_{76} and 2Cr-$B_{38}N_{38}$ nanocages and G_{specie} is free Gibbs energies of intermediates of CO_2 reduction reactions and the $G_{specie\text{-}nanocage}$ is free Gibbs energies of complexes of 2Cr-Si_{76}, 2Cr-C_{76} and 2Cr-$B_{38}N_{38}$ nanocages with intermediates of CO_2 reduction reactions [19].

The $\Delta G_{reaction}$ of reaction steps of CO_2 reduction reactions on 2Cr-Si_{76}, 2Cr-C_{76} and Cr2-$B_{38}N_{38}$ are calculated [20-23]:

$$\Delta G_{reaction} = \Delta E + \Delta ZPE - T\Delta S + eU + \Delta G_{pH} \quad (2)$$

The T, E, S and ZPE are temperature, energy, entropy and zero-point energy of complexes of Si_{76}, C_{76}, $B_{38}N_{38}$, 2Cr-Si_{76}, 2Cr-C_{76} and 2Cr-$B_{38}N_{38}$ with species [24]. The ΔG_{pH} as free energy correction because of variations in H^+ concentration can be calculated by $G_{pH} = -kT \ln [H^+] = kT \ln 10 \times pH$, and pH is 0. The U and *e* are applied potential and number of electron transfer, respectively [24]. The U is potential of electrode commissioned to electrode of standard hydrogen and the values of U is started since 0 until 1.23 V in balance potential U_0 and several stages of CO_2-RR are formidable. The used potential U is requested to eliminate positive part of Gibbs free energy and overvoltage is defined as $\eta = U_0 - U$ [24, 25]. The zero-point energy and entropy contributions of nanocages (Si_{76}, C_{76} and $B_{38}N_{38}$), metal doped nanocages (2Cr-Si_{76}, 2Cr-C_{76} and 2Cr-$B_{38}N_{38}$) and their complexes of intermediates of reaction steps of CO_2-RR on 2Cr-Si_{76}, 2Cr-C_{76} and 2Cr-$B_{38}N_{38}$ have been calculated by vibrational frequencies of optimized structures by M06-2X /6-311+G (2d, 2p) method [17-20].

Results and Discussion

Nanocages (Si_{76}, C_{76} and $B_{38}N_{38}$ and 2Cr-Si_{76}, 2Cr-C_{76} and 2Cr-$B_{38}N_{38}$)

The properties of Si_{76}, C_{76} and $B_{38}N_{38}$ nanocages and 2Cr-doped structures (2Cr-Si_{76}, 2Cr-C_{76} and 2Cr-$B_{38}N_{38}$) are investigated. The Si_{76}, C_{76}, $B_{38}N_{38}$, 2Cr-Si_{76}, 2Cr-C_{76} and 2Cr-$B_{38}N_{38}$ nanocages are presented in Figure 1. The $\Delta G_{adsorption}$ [25-28] values of Cr on Si_{76}, C_{76} and $B_{38}N_{38}$ are examined in Table 1:

$$\Delta G_{adsorption} = G_{2Cr\text{-}nanocage} - G_{nanocage} - 2G_{Cr} \quad (3)$$

The $G_{nanocage}$ is free Gibbs energies of Si_{76}, C_{76} and $B_{38}N_{38}$ nanocages and G_{Cr} is free Gibbs energy of Cr and $G_{2Cr\text{-}nanocage}$ is free Gibbs energies of Cr with Si_{76}, C_{76} and $B_{38}N_{38}$. The $\Delta G_{adsorption}$ of 2Cr-Si_{76}, 2Cr-C_{76} and 2Cr-$B_{38}N_{38}$ nanocages are -6.79, -6.21 and -6.46 eV. The 2Cr-Si_{76} and 2Cr-$B_{38}N_{38}$ nanocages have higher $\Delta G_{adsorption}$ than 2Cr-C_{76} nanocage. The $\Delta G_{adsorption}$ of 2Cr-C_{76} nanocage are lower than 2Cr-Si_{76} and 2Cr-$B_{38}N_{38}$ nanocages ca 0.51 and 0.25 eV. The values of $\Delta G_{adsorption}$ for Cr on Si_{76}, C_{76} and $B_{38}N_{38}$ are all negative pointing out that this process is exothermic.

The formation energies ($\Delta E_{formation}$) of Si_{76}, C_{76} and $B_{38}N_{38}$ nanocages and 2Cr-Si_{76}, 2Cr-C_{76} and 2Cr-$B_{38}N_{38}$ are examined [29] in Table 1:

$$\Delta E_{formation} = E_{nanocage} - 76 * E_X \quad (4)$$

$$\Delta E_{formation} = E_{2Cr\text{-}nanocage} - E_{nanocage} - 2*E_{Cr} \quad (5)$$

The $E_{2Cr\text{-}nanocage}$ is energies of Cr with 2Cr-Si_{76}, 2Cr-C_{76} and 2Cr-$B_{38}N_{38}$, the $E_{nanocage}$ is energies of nanocages, the E_{Cr} is energy of Cr atom and E_X is energies of Si, C and BN. The $\Delta E_{formation}$ of 2Cr-Si_{76}, 2Cr-C_{76} and 2Cr-$B_{38}N_{38}$ nanocages are -5.25, -4.95 and -5.19 eV. The 2Cr-Si_{76} and 2Cr-$B_{38}N_{38}$ nanocages have higher $\Delta E_{formation}$ than 2Cr-C_{76} nanocage. In this study, the relative energy for acceptable spin states and spin multiplicities (S = 3, 2 and 1 and 2S+1 = 7, 5 and 3) of Cr atoms in 2Cr-Si_{76}, 2Cr-C_{76} and 2Cr-$B_{38}N_{38}$ are reported in Table 2. The $\Delta E_{formation}$ of 2Cr-C_{76} nanocage is lower than 2Cr-Si_{76} and 2Cr-$B_{38}N_{38}$ nanocages ca 0.31 and 0.23 eV. The values of $\Delta E_{formation}$ of Si_{76}, C_{76}, $B_{38}N_{38}$, 2Cr-Si_{76}, 2Cr-C_{76} and 2Cr-$B_{38}N_{38}$ are all negative. The $\Delta E_{formation}$ of Si and BN nanocages are higher than C nanocages.

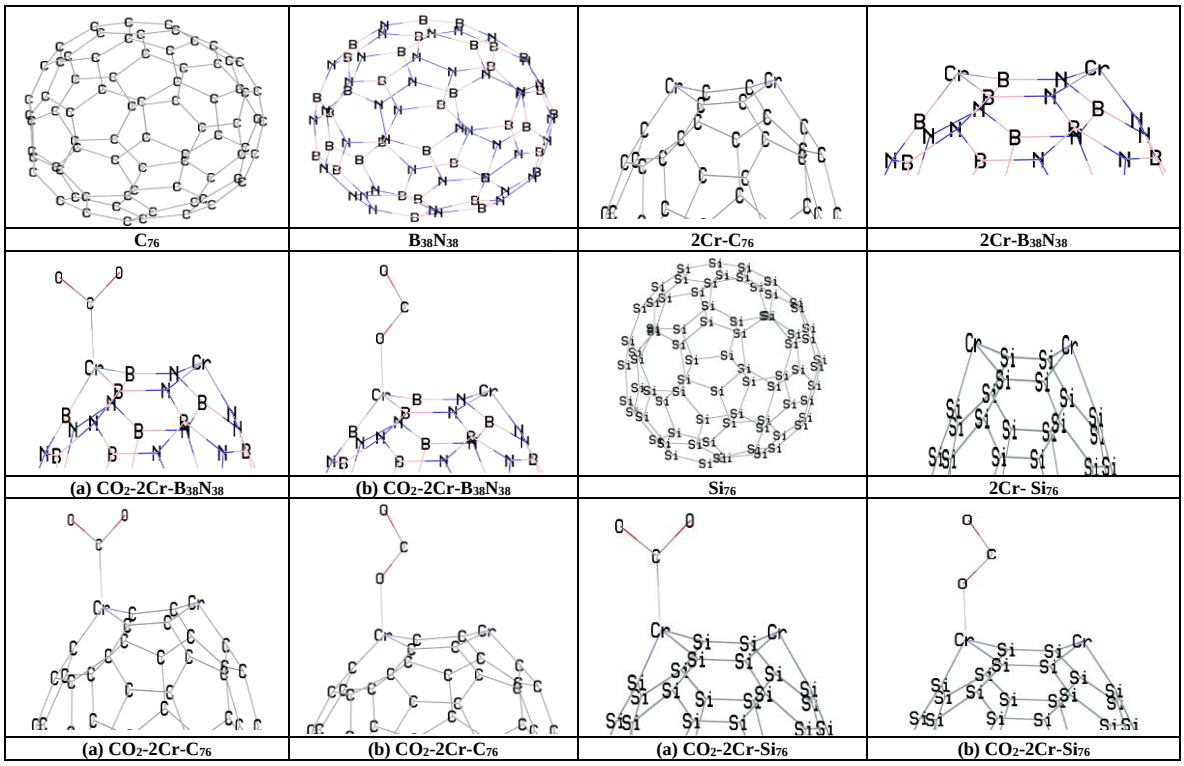

Fig. 1: Structures of Si_{76}, C_{76} and $B_{38}N_{38}$ nanocages, 2Cr-Si_{76}, 2Cr-C_{76} and 2Cr-$B_{38}N_{38}$ nanocages and complexes with CO_2.

Table-1: The $\Delta E_{formation}$ and $\Delta G_{adsorption}$ of 2Cr-Si_{76}, 2Cr-C_{76} and 2Cr-$B_{38}N_{38}$ nanocages, the $\Delta G_{adsorption}$ of CO_2 reduction reactions on 2Cr-Si_{76}, 2Cr-C_{76} and 2Cr-$B_{38}N_{38}$ nanocages.

M06-2X/6-311+G (2d, 2p)			
Nanocages	**2Cr-C_{76}**	**2Cr-$B_{38}N_{38}$**	**2Cr-Si_{76}**
$\Delta E_{formation}$	**-4.95**	**-4.95**	**-5.19**
$\Delta G_{adsorption}$	**-6.21**	**-6.21**	**-6.46**
$\Delta G_{adsorption}$	**2Cr-C_{76}**	**2Cr-$B_{38}N_{38}$**	**2Cr-Si_{76}**
CO_2 (a)	**-0.99**	**-1.07**	**-1.20**
CO_2 (b)	**-0.90**	**-0.97**	**-1.09**
CO	**-2.81**	**-3.03**	**-3.41**
HCOOH	**-1.60**	**-1.73**	**-1.95**
HCHO	**-2.00**	**-2.16**	**-2.43**
CH_3OH	**-1.73**	**-1.86**	**-2.09**
CH_4	**-0.85**	**-0.92**	**-1.04**
PBEPBE/6-311+G (2d, 2p)			
Nanocages	**2Cr-C_{76}**	**2Cr-$B_{38}N_{38}$**	**2Cr-Si_{76}**
$\Delta E_{formation}$	**-4.89**	**-4.86**	**-5.10**
$\Delta G_{adsorption}$	**-6.10**	**-6.10**	**-6.34**
$\Delta G_{adsorption}$	**2Cr-C_{76}**	**2Cr-$B_{38}N_{38}$**	**2Cr-Si_{76}**
CO_2 (a)	**-0.97**	**-1.05**	**-1.18**
CO_2 (b)	**-0.88**	**-0.95**	**-1.07**
CO	**-2.76**	**-2.98**	**-3.35**
HCOOH	**-1.57**	**-1.70**	**-1.91**
HCHO	**-1.96**	**-2.12**	**-2.39**
CH_3OH	**-1.70**	**-1.83**	**-2.05**
CH_4	**-0.83**	**-0.90**	**-1.02**
B3LYP-D3/6-311+G (2d, 2p)			
Nanocages	**2Cr-C_{76}**	**2Cr-$B_{38}N_{38}$**	**2Cr-Si_{76}**
$\Delta E_{formation}$	**-4.92**	**-4.92**	**-5.15**
$\Delta G_{adsorption}$	**-6.17**	**-6.17**	**-6.41**
$\Delta G_{adsorption}$	**2Cr-C_{76}**	**2Cr-$B_{38}N_{38}$**	**2Cr-Si_{76}**
CO_2 (a)	**-0.98**	**-1.06**	**-1.18**
CO_2 (b)	**-0.89**	**-0.96**	**-1.07**
CO	**-2.77**	**-2.99**	**-3.36**
HCOOH	**-1.58**	**-1.71**	**-1.92**
HCHO	**-1.97**	**-2.13**	**-2.40**
CH_3OH	**-1.71**	**-1.83**	**-2.06**
CH_4	**-0.84**	**-0.91**	**-1.03**

CO_2-RR to CO, CH_4, HCOOH, HCHO and CH_3OH on surfaces of 2Cr-Si_{76}, 2Cr-C_{76} and 2Cr-$B_{38}N_{38}$ nanocages

In this section the potential of 2Cr-Si_{76}, 2Cr-C_{76} and 2Cr-$B_{38}N_{38}$ nanocages to catalyze the CO_2-RR to CH_4 and CH_3OH is investigated. The three mechanisms for CO_2-RR (Pathway 1: $*CO_2 \rightarrow *COOH \rightarrow *CO \rightarrow *CHO \rightarrow *CH_2O \rightarrow *CH_3O \rightarrow CH_3OH \rightarrow *O + CH_4$; Pathway 2: $*CO_2 \rightarrow *OCHO \rightarrow$ *-HCOOH $\rightarrow *CHO \rightarrow *HCHO$ and Pathway 3: $*CO2 \rightarrow *COOH \rightarrow$ *-HCOOH) are investigated. The adsorption of CO_2 on 2Cr-Si_{76}, 2Cr-C_{76} and 2Cr-$B_{38}N_{38}$ is investigated. The structures of complexes of CO_2 on 2Cr-Si_{76}, 2Cr-C_{76} and 2Cr-$B_{38}N_{38}$ nanocages are presented in Figure 1. The calculated $\Delta G_{adsorption}$ of CO_2 on 2Cr-Si_{76}, 2Cr-C_{76} and 2Cr-$B_{38}N_{38}$ are summarized in Table 1.

The $\Delta G_{adsorption}$ of CO_2 on 2Cr-Si_{76}, 2Cr-C_{76} and 2Cr-$B_{38}N_{38}$ nanocages via position *a* are -1.20, -0.99 and -1.07 eV. The $\Delta G_{adsorption}$ of CO_2 on 2Cr-Si_{76}, 2Cr-C_{76} and 2Cr-$B_{38}N_{38}$ nanocages via position *b* are -1.09, -0.90 and -0.97 eV. The Cr atoms of 2Cr-Si_{76}, 2Cr-C_{76} and 2Cr-$B_{38}N_{38}$ nanocages is adsorbed the CO_2 by O and C. The $\Delta G_{adsorption}$ of CO_2 on 2Cr-C_{76} nanocage via positons *a* and *b* are lower than 2Cr-Si_{76} and 2Cr-$B_{38}N_{38}$ nanocages ca 0.19 and 0.08 eV. The $\Delta G_{adsorption}$ of CO_2 on 2Cr-Si_{76}, 2Cr-C_{76} and 2Cr-$B_{38}N_{38}$ nanocages via positon *a* are higher than positon *b* ca 0.09 to 0.11 eV. The 2Cr-Si_{76} and 2Cr-$B_{38}N_{38}$ nanocages have higher $\Delta G_{adsorption}$ than 2Cr-C_{76} nanocage [30-32]. The structures of CO_2-RR to create the CO, CH_4, HCOOH, HCHO and CH_3OH on 2Cr-Si_{76}, 2Cr-C_{76} and 2Cr-$B_{38}N_{38}$ are presented in Figure 2. In this study, the relative energy for acceptable spin states and spin multiplicities (S = 3, 2 and 1 and 2S+1 = 7, 5 and 3) of Cr atoms in complexes of 2Cr-Si_{76}, 2Cr-C_{76} and 2Cr-$B_{38}N_{38}$ with intermediates of reaction steps of CO2-RR are reported in Table-2.

The $\Delta G_{reaction}$ and $E_{barrier}$ of reaction steps of CO_2-RR on 2Cr-Si_{76}, 2Cr-C_{76} and 2Cr-$B_{38}N_{38}$ nanocages are presented in Table 3. After adsorption of CO_2 on 2Cr-Si_{76}, 2Cr-C_{76} and 2Cr-$B_{38}N_{38}$ nanocages is CO_2 protonation to create the nanocage-*COOH and nanocage-*OCHO [33, 34]. The $\Delta G_{reaction}$ of formation of nanocage-*OCHO on 2Cr-Si_{76}, 2Cr-C_{76} and 2Cr-$B_{38}N_{38}$ nanocages are -0.44, -0.36 and -0.39 eV. The $E_{barrier}$ of formation of nanocage-*OCHO on 2Cr-Si_{76}, 2Cr-C_{76} and 2Cr-$B_{38}N_{38}$ nanocages are 0.23, 0.26 and 0.24 eV. The $\Delta G_{reaction}$ of formation of nanocage-*COOH on 2Cr-Si_{76}, 2Cr-C_{76} and 2Cr-$B_{38}N_{38}$ nanocages are -0.35, -0.28 and -0.31 eV. The $E_{barrier}$ of formation of nanocage-*COOH on 2Cr-Si_{76}, 2Cr-C_{76} and 2Cr-$B_{38}N_{38}$ nanocages are 0.15, 0.17 and 0.16 eV.

The $E_{barrier}$ of nanocage-*OCHO is higher than nanocage-*COOH on 2Cr-Si_{76}, 2Cr-C_{76} and 2Cr-$B_{38}N_{38}$ nanocages. The $\Delta G_{reaction}$ of *OCHO is more negative than *COOH on 2Cr-Si_{76}, 2Cr-C_{76} and 2Cr-$B_{38}N_{38}$ nanocages and the *COOH and *OCHO are created to other possible species. The *CO is produced from *COOH on 2Cr-Si_{76}, 2Cr-C_{76} and 2Cr-$B_{38}N_{38}$. The CO desorption is required high $\Delta G_{reaction}$ and CO production has low efficiency on 2Cr-Si_{76}, 2Cr-C_{76} and 2Cr-$B_{38}N_{38}$. The $\Delta G_{reaction}$ of formation of nanocage-*CO on 2Cr-Si_{76}, 2Cr-C_{76} and 2Cr-$B_{38}N_{38}$ nanocages are -0.37, -0.30 and -0.32 eV. The $E_{barrier}$ of formation of nanocage-*CO on 2Cr-Si_{76}, 2Cr-C_{76} and 2Cr-$B_{38}N_{38}$ nanocages are 0.23, 0.26 and 0.24 eV. The *COOH and *OCHO on 2Cr-Si_{76}, 2Cr-C_{76} and 2Cr-$B_{38}N_{38}$ are converted to HCOOH.

Table-2: The relative energy in eV of 2Cr-Si_{76}, 2Cr-C_{76} and 2Cr-$B_{38}N_{38}$ nanocages (S = 3, 2 and 1 and 2S+1 = 7, 5 and 3) and their complexes with intermediates of CO_2 reduction reactions.

Relative energy	**2Cr-C_{76}**			**2Cr-$B_{38}N_{38}$**			**2Cr-Si_{76}**		
S	**1**	**2**	**3**	**1**	**2**	**3**	**1**	**2**	**3**
2S + 1	**3**	**5**	**7**	**3**	**5**	**7**	**3**	**5**	**7**
Relative energy	**0.0452**	**0.0283**	**0.000**	**0.0416**	**0.0237**	**0.000**	**0.0473**	**0.0266**	**0.000**
Complexes		**2Cr-C_{76}**			**2Cr-$B_{38}N_{38}$**			**2Cr-Si_{76}**	
S	**1**	**2**	**3**	**1**	**2**	**3**	**1**	**2**	**3**
2S + 1	**3**	**5**	**7**	**3**	**5**	**7**	**3**	**5**	**7**
CO_2 (a)	**0.0450**	**0.0280**	**0.0000**	**0.0410**	**0.0230**	**0.0000**	**0.0470**	**0.0260**	**0.0000**
CO_2 (b)	**0.0444**	**0.0276**	**0.0000**	**0.0405**	**0.0227**	**0.0000**	**0.0464**	**0.0257**	**0.0000**
CO	**0.0415**	**0.0258**	**0.0000**	**0.0378**	**0.0212**	**0.0000**	**0.0433**	**0.0240**	**0.0000**
HCOOH	**0.0403**	**0.0251**	**0.0000**	**0.0367**	**0.0206**	**0.0000**	**0.0421**	**0.0233**	**0.0000**
HCHO	**0.0389**	**0.0242**	**0.0000**	**0.0354**	**0.0199**	**0.0000**	**0.0406**	**0.0225**	**0.0000**
CHO	**0.0374**	**0.0233**	**0.0000**	**0.0341**	**0.0191**	**0.0000**	**0.0391**	**0.0216**	**0.0000**
CH_2O	**0.0356**	**0.0221**	**0.0000**	**0.0324**	**0.0182**	**0.0000**	**0.0371**	**0.0205**	**0.0000**
CH_3O	**0.0351**	**0.0218**	**0.0000**	**0.0320**	**0.0179**	**0.0000**	**0.0367**	**0.0203**	**0.0000**
CH_3OH	**0.0331**	**0.0206**	**0.0000**	**0.0302**	**0.0169**	**0.0000**	**0.0346**	**0.0191**	**0.0000**
CH_4	**0.0305**	**0.0190**	**0.0000**	**0.0278**	**0.0156**	**0.0000**	**0.0318**	**0.0176**	**0.0000**

Table-3: The $E_{activation}$, $\Delta G_{reaction}$ in eV of CO_2-RR on 2Cr-Si_{76}, 2Cr-C_{76} and 2Cr-$B_{38}N_{38}$ nanocages.

M06-2X/6-311+G (2d, 2p)						
Nanocages	**2Cr-C_{76}**		**2Cr-$B_{38}N_{38}$**		**2Cr-Si_{76}**	
CO_2 reduction reaction	**$E_{activation}$**	**$\Delta G_{reaction}$**	**$E_{activation}$**	**$\Delta G_{reaction}$**	**$E_{activation}$**	**$\Delta G_{reaction}$**
***CO_2 → *COOH**	0.17	-0.28	0.16	-0.31	0.15	-0.35
***COOH → *CO**	0.26	-0.30	0.24	-0.32	0.23	-0.37
***CO → *CHO**	0.14	0.27	0.13	0.29	0.12	0.33
***CHO → *CH_2O**	0.27	0.24	0.25	0.26	0.24	0.30
***CH_2O → *CH_3O**	0.13	-0.43	0.12	-0.47	0.11	-0.53
***CH_3O → CH_3OH**	0.40	-0.66	0.37	-0.71	0.35	-0.81
***CH_3O → *O + CH_4**	0.28	-1.38	0.26	-1.48	0.25	-1.70
***COOH → *-HCOOH**	0.47	0.19	0.43	0.21	0.41	0.23
***CO_2 → *OCHO**	0.26	-0.36	0.24	-0.39	0.23	-0.44
***OCHO → *-HCOOH**	0.38	-0.08	0.35	-0.09	0.33	-0.10
***HCOOH → *CHO**	0.51	-0.13	0.48	-0.13	0.46	-0.16
***CHO → *HCHO**	0.36	-0.64	0.34	-0.69	0.32	-0.79
PBEPBE/6-311+G (2d, 2p)						
***CO_2 → *COOH**	0.16	-0.29	0.15	-0.32	0.14	-0.36
***COOH → *CO**	0.25	-0.31	0.23	-0.33	0.22	-0.38
***CO → *CHO**	0.13	0.28	0.12	0.30	0.11	0.34
***CHO → *CH_2O**	0.26	0.25	0.24	0.27	0.23	0.31
***CH_2O → *CH_3O**	0.12	-0.44	0.11	-0.49	0.10	-0.55
***CH_3O → CH_3OH**	0.38	-0.68	0.35	-0.73	0.33	-0.84
***CH_3O → *O + CH_4**	0.26	-1.43	0.25	-1.53	0.24	-1.76
***COOH → *-HCOOH**	0.44	0.20	0.41	0.22	0.39	0.24
***CO_2 → *OCHO**	0.25	-0.37	0.23	-0.40	0.22	-0.46
***OCHO → *-HCOOH**	0.36	-0.08	0.33	-0.09	0.31	-0.10
***HCOOH → *CHO**	0.48	-0.13	0.45	-0.13	0.43	-0.17
***CHO → *HCHO**	0.34	-0.66	0.32	-0.71	0.30	-0.82
B3LYP-D3/6-311+G (2d, 2p)						
***CO_2 → *COOH**	0.16	-0.29	0.15	-0.32	0.14	-0.37
***COOH → *CO**	0.24	-0.31	0.22	-0.33	0.22	-0.39
***CO → *CHO**	0.13	0.28	0.12	0.30	0.11	0.34
***CHO → *CH_2O**	0.25	0.25	0.23	0.27	0.22	0.31
***CH_2O → *CH_3O**	0.12	-0.45	0.11	-0.49	0.10	-0.55
***CH_3O → CH_3OH**	0.37	-0.69	0.35	-0.74	0.33	-0.85
***CH_3O → *O + CH_4**	0.26	-1.44	0.24	-1.55	0.23	-1.78
***COOH → *-HCOOH**	0.44	0.20	0.40	0.22	0.38	0.24
***CO_2 → *OCHO**	0.24	-0.38	0.22	-0.41	0.22	-0.46
***OCHO → *-HCOOH**	0.36	-0.08	0.33	-0.09	0.31	-0.10
***HCOOH → *CHO**	0.48	-0.14	0.45	-0.14	0.43	-0.17
***CHO → *HCHO**	0.34	-0.67	0.32	-0.72	0.30	-0.83

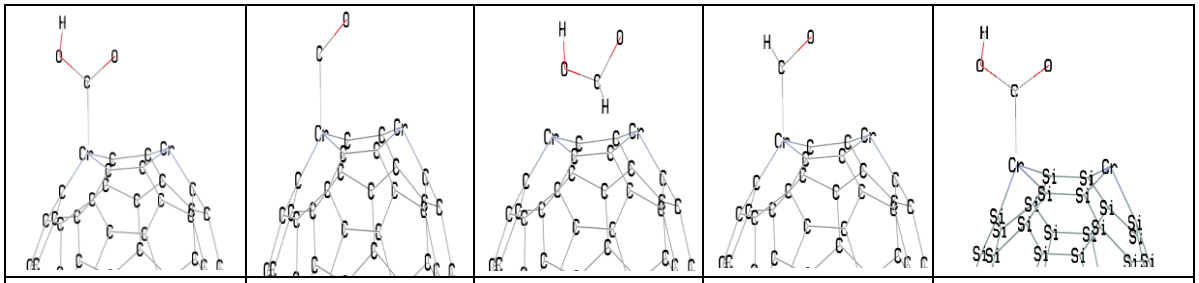

HOOC-2Cr-C_{76}	**OC-2Cr-C_{76}**	**HOOCH-2Cr-C_{76}**	**OCH-2Cr-C_{76}**	**HOOC-2Cr-Si_{76}**
OCH_2-2Cr-C_{76}	**OCH_3-2Cr-C_{76}**	**$HOCH_3$-2Cr-C_{76}**	**CH_4-2Cr-C_{76}**	**OHCO-2Cr-C_{76}**

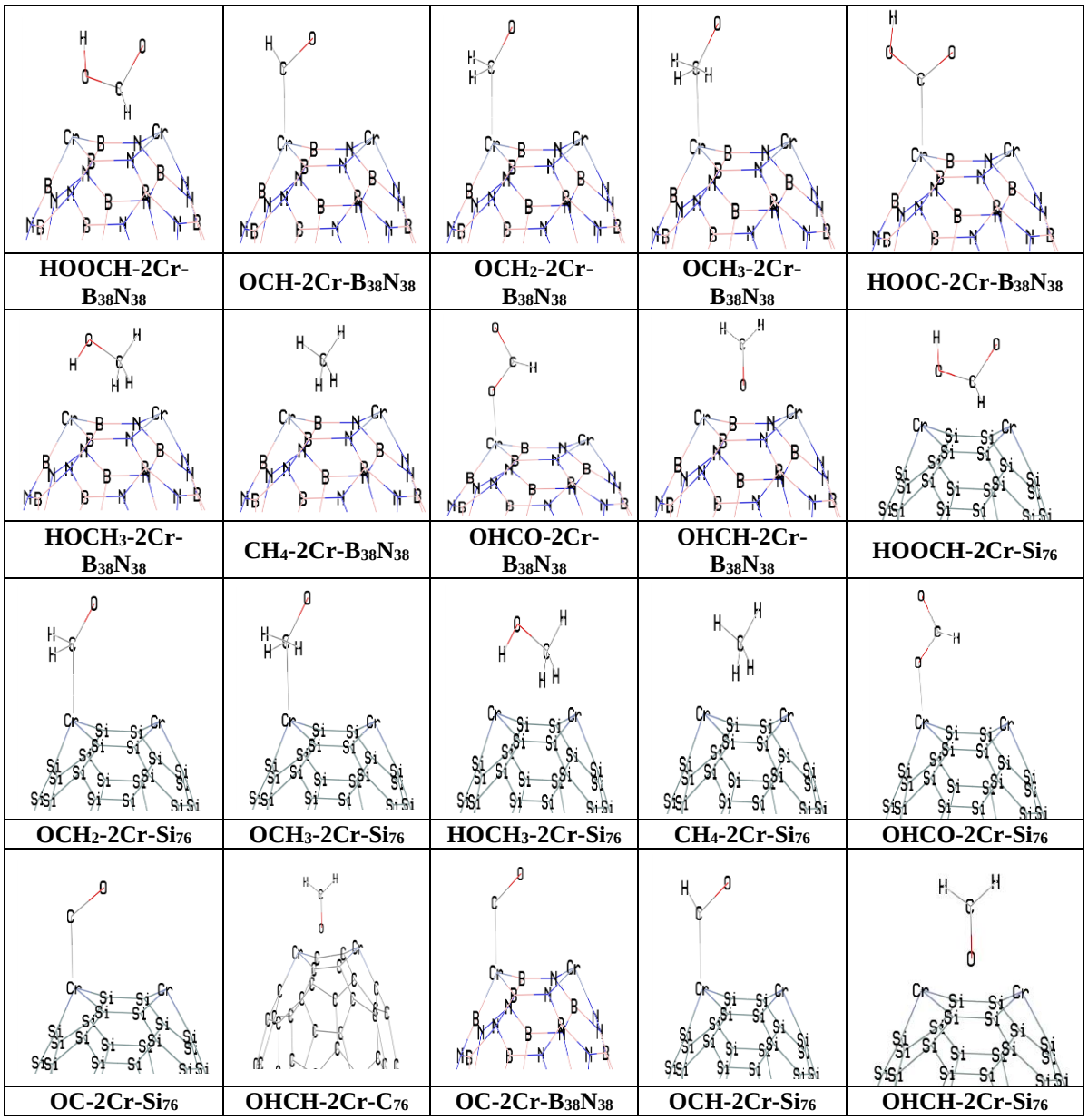

Fig. 2: Structures of complexes of CO_2-RR derivatives with 2Cr-Si_{76}, 2Cr-C_{76} and 2Cr-$B_{38}N_{38}$ nanocages.

The $\Delta G_{reaction}$ values of reaction steps of CO_2-RR (Pathway 1: $*CO_2 \rightarrow *COOH \rightarrow *CO \rightarrow *CHO \rightarrow *CH_2O \rightarrow *CH_3O \rightarrow CH_3OH \rightarrow *O + CH_4$; Pathway 2: $*CO_2 \rightarrow *OCHO \rightarrow *\text{-}HCOOH \rightarrow *CHO \rightarrow *HCHO$ and Pathway 3: $*CO_2 \rightarrow *COOH \rightarrow *\text{-}HCOOH$) on 2Cr-$Si_{76}$, 2Cr-$C_{76}$ and 2Cr-$B_{38}N_{38}$ nanocages are presented in Figures 3, and the Gibbs free energy plan of reaction steps of CO_2-RR on 2Cr-Si_{76}, 2Cr-C_{76} and 2Cr-$B_{38}N_{38}$ nanocages in various U values are presented in Figures 4. The $*CO_2 \rightarrow *OCHO \rightarrow HCOOH$ reactions is favored pathway and $\Delta G_{reaction}$ of formation of nanocage-*OCHO on 2Cr-Si_{76}, 2Cr-C_{76} and 2Cr-$B_{38}N_{38}$ nanocages are -0.44, -0.36 and -0.39 eV. The $E_{barrier}$ of formation of nanocage-*OCHO on 2Cr-Si_{76}, 2Cr-C_{76} and 2Cr-$B_{38}N_{38}$ nanocages are 0.23, 0.26 and 0.24 eV. The CO and HCOOH creation on 2Cr-$B_{38}N_{38}$ have higher $\Delta G_{reaction}$ and lower $E_{barrier}$ than 2Cr-Si_{76} and 2Cr-C_{76}. The $*COOH \rightarrow *CO + H_2O$ is rate-limiting on 2Cr-Si_{76}, 2Cr-C_{76} and 2Cr-$B_{38}N_{38}$ nanocages.

Pathway 1: *CO_2 (0) → *COOH (2) → *CO (4) → *CHO (6) → *CH_2O (8) → *CH_3O (10) → CH_3OH (12) → *O + CH_4 (14)

Pathway 2: *CO_2 → *OCHO → *-HCOOH → *CHO → *HCHO

Pathway 3: *CO_2 → *COOH → *-HCOOH

2Cr-C_{76}

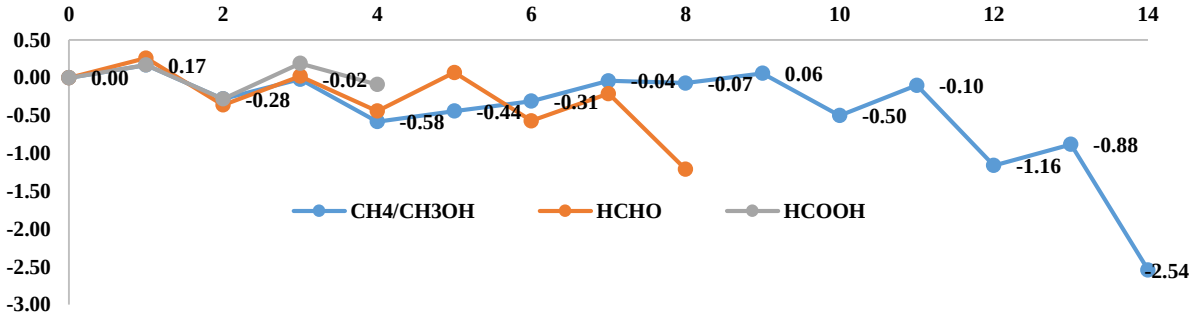

2Cr-$B_{38}N_{38}$

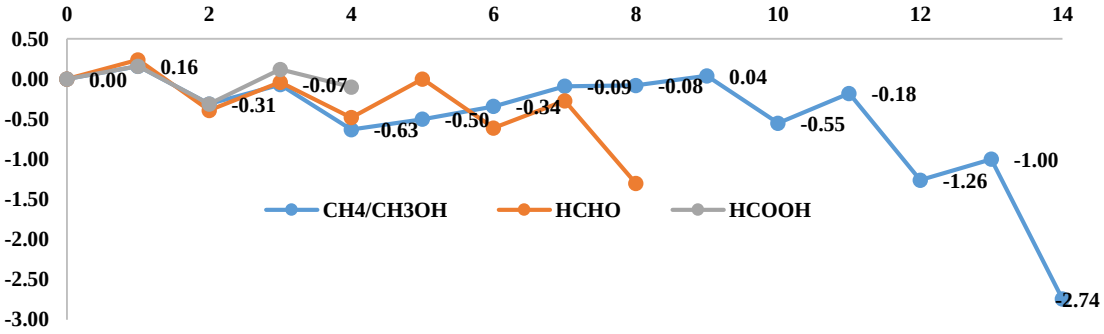

2Cr-Si_{76}

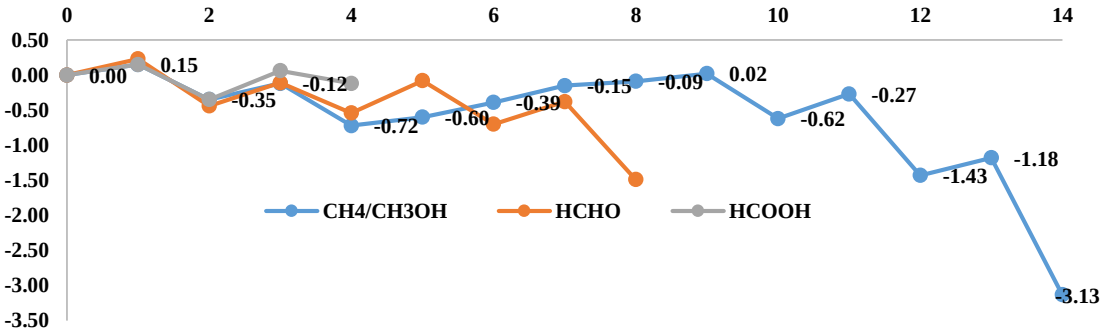

Fig. 3: The $\Delta G_{reaction}$ of reaction steps of CO_2-RR on 2Cr-Si_{76}, 2Cr-C_{76} and 2Cr-$B_{38}N_{38}$ nanocages.

The CH_3OH creation on 2Cr-Si_{76}, 2Cr-C_{76} and 2Cr-$B_{38}N_{38}$ is done by acceptable pathways and *CO → *CHO is rate limiting on 2Cr-Si_{76}, 2Cr-C_{76} and 2Cr-$B_{38}N_{38}$. The values of $\Delta G_{reaction}$ of CH_3OH creation on 2Cr-Si_{76} and 2Cr-$B_{38}N_{38}$ nanocages are more negative than 2Cr-C_{76} nanocage. The $\Delta G_{reaction}$ of formation of nanocage-*CH_3O on 2Cr-Si_{76}, 2Cr-C_{76} and 2Cr-$B_{38}N_{38}$ nanocages are -0.53, -0.43 and -0.47 eV. The $E_{barrier}$ of formation of nanocage-*CH_3O on 2Cr-Si_{76}, 2Cr-C_{76} and 2Cr-$B_{38}N_{38}$ nanocages are 0.11, 0.13 and 0.12 eV. The reaction of CH_3OH creation on 2Cr-Si_{76} and 2Cr-$B_{38}N_{38}$ nanocages have lower $E_{barrier}$ than 2Cr-C_{76} nanocage, significantly.

The HCHO creation on 2Cr-Si_{76}, 2Cr-C_{76} and 2Cr-$B_{38}N_{38}$ nanocages is processed. The *CO → *CHO is rate-limiting of HCHO production on 2Cr-Si_{76}, 2Cr-C_{76} and 2Cr-$B_{38}N_{38}$ nanocages. The $\Delta G_{reaction}$ of formation of nanocage-*CHO on 2Cr-Si_{76}, 2Cr-C_{76} and 2Cr-$B_{38}N_{38}$ nanocages are 0.33, 0.27 and 0.29 eV. The $E_{barrier}$ of formation of nanocage-*CHO on 2Cr-Si_{76}, 2Cr-C_{76} and 2Cr-$B_{38}N_{38}$ nanocages are 0.12, 0.14 and 0.13 eV. The CO_2 is hydrogenated on 2Cr-Si_{76}, 2Cr-C_{76} and 2Cr-$B_{38}N_{38}$ and CH_4 is created and rate limiting is the *CO → *CHO.

Results shown that the *CH_3O → CH_3OH reaction step for CO_2-RR via pathway 1 (*CO_2 → *COOH → *CO → *CHO → *CH_2O → *CH_3O → CH_3OH → *O + CH_4) on 2Cr-Si_{76}, 2Cr-C_{76} and 2Cr-$B_{38}N_{38}$ is the rate-limiting step for CO_2-RR via pathway 1. The *HCOOH → *CHO reaction step for CO_2-RR via pathway 2 (*CO_2 → *OCHO → *-HCOOH → *CHO → *HCHO) on 2Cr-Si_{76}, 2Cr-C_{76} and 2Cr-$B_{38}N_{38}$ is the rate-limiting step for CO_2-RR via pathway 2. The *COOH → *-HCOOH reaction step for CO_2-RR via pathway 3 (*CO_2 → *COOH → *-HCOOH) on 2Cr-Si_{76}, 2Cr-C_{76} and 2Cr-$B_{38}N_{38}$ is the rate-limiting step for CO_2-RR via pathway 3.

The over-potential for CO, HCOOH, HCHO, CH_3OH and CH_4 production via Metal-based catalysts (Fe, Ni and Co single atom as catalysts, Cu, Au, Ag based bimetallic catalysts and Pt and Pd as metal catalysts) in previous works [11-15] are summarized in Table 4. The over-potential for CO, HCOOH, HCHO, CH_3OH and CH_4 production on 2Cr-Si_{76}, 2Cr-C_{76} and 2Cr-$B_{38}N_{38}$ nanocages are reported in Table 4. The over-potential for CO, HCOOH, HCHO, CH_3OH and CH_4 production on 2Cr-Si_{76} nanocage is 0.30, 0.24, 0.27, 0.21 and 0.19 V. The over-potential for CH_4 and CH_3OH formation are lower than HCOOH on 2Cr-Si_{76}, 2Cr-C_{76} and 2Cr-$B_{38}N_{38}$ nanocages. The over-potential for CO, HCOOH, HCHO, CH_3OH and CH_4 production on 2Cr-C_{76} nanocage is 0.36, 0.30, 0.33, 0.26 and 0.24 V. The over-potential for CO, CH_4, HCOOH, HCHO and CH_3OH on 2Cr-Si_{76} and 2Cr-$B_{38}N_{38}$ nanocages are lower than 2Cr-C_{76} nanocage. The over-potential of CO_2-RR on 2Cr-C_{76} and 2Cr-$B_{38}N_{38}$ are lower than Fe, Ni and Co single atom as catalysts, Cu, Au, Ag based bimetallic catalysts and Pt and Pd as metal catalysts in previous works [11-15]. The over-potential for CO, HCOOH, HCHO, CH_3OH and CH_4 production on 2Cr-$B_{38}N_{38}$ nanocage is 0.34, 0.27, 0.31, 0.24 and 0.22 V. The 2Cr-Si_{76}, 2Cr-C_{76} and 2Cr-$B_{38}N_{38}$ are catalyzed the CO_2-RR to create the CO, CH_4, HCOOH, HCHO and CH_3OH with acceptable performance.

Table-4: The over-potential in V of CO_2-RR on 2Cr-Si_{76}, 2Cr-C_{76} and 2Cr-$B_{38}N_{38}$ nanocages and reported over-potential in V of CO_2-RR on Metal-based catalysts in previous works [11-15].

M06-2X			
Overpotential	**2Cr-C_{76}**	**2Cr-$B_{38}N_{38}$**	**2Cr-Si_{76}**
CO production	**0.36**	**0.34**	**0.30**
HCOOH production	**0.30**	**0.27**	**0.24**
HCHO production	**0.33**	**0.31**	**0.27**
CH_3OH production	**0.26**	**0.24**	**0.21**
CH_4 production	**0.24**	**0.22**	**0.19**
PBEPBE			
Overpotential	**2Cr-C_{76}**	**2Cr-$B_{38}N_{38}$**	**2Cr-Si_{76}**
CO production	**0.34**	**0.32**	**0.28**
HCOOH production	**0.28**	**0.25**	**0.22**
HCHO production	**0.31**	**0.29**	**0.25**
CH_3OH production	**0.24**	**0.22**	**0.20**
CH_4 production	**0.22**	**0.21**	**0.18**
B3LYP-D3			
Overpotential	**2Cr-C_{76}**	**2Cr-$B_{38}N_{38}$**	**2Cr-Si_{76}**
CO production	**0.33**	**0.31**	**0.27**
HCOOH production	**0.27**	**0.25**	**0.22**
HCHO production	**0.30**	**0.28**	**0.25**
CH_3OH production	**0.24**	**0.22**	**0.19**
CH_4 production	**0.22**	**0.20**	**0.17**
Metal-based catalysts in previous works [11-15]			
Overpotential	**Fe, Ni and Co single atom as catalysts**	**Cu, Au, Ag based bimetallic catalysts**	**Pt and Pd as metal catalysts**
CO production	**0.38**	**0.40**	**0.37**
HCOOH production	**0.31**	**0.34**	**0.30**
HCHO production	**0.35**	**0.37**	**0.34**
CH_3OH production	**0.27**	**0.29**	**0.27**
CH_4 production	**0.25**	**0.27**	**0.25**

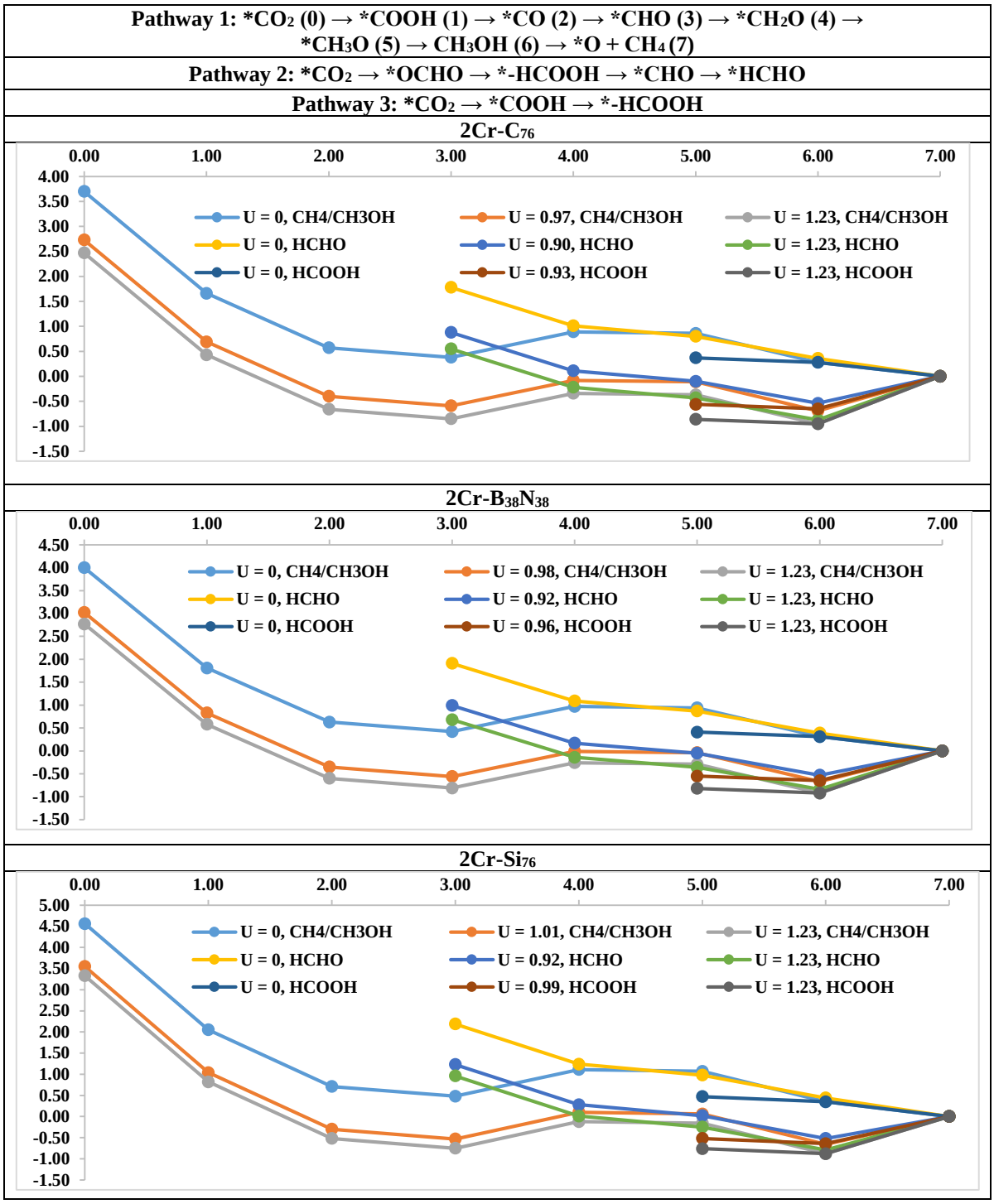

Fig. 4: The Gibbs free energy plan of reaction steps of CO_2-RR on 2Cr-Si_{76}, 2Cr-C_{76} and 2Cr-$B_{38}N_{38}$ nanocages in various U values.

Conclusion

The capacities of 2Cr-Si_{76}, 2Cr-C_{76} and 2Cr-$B_{38}N_{38}$ as catalysts for CO_2-RR to produce the CH_4 and CH_3OH are investigated. The $\Delta G_{reaction}$ of CO_2-RR to create CH_4 and CH_3OH on 2Cr-Si_{76}, 2Cr-C_{76} and 2Cr-$B_{38}N_{38}$ are calculated. The limiting step of creation of CH_4 and CH_3OH is *CO → *CHO on 2Cr-Si_{76}, 2Cr-C_{76} and 2Cr-$B_{38}N_{38}$. The over-potential for CO, HCOOH, HCHO, CH_3OH and CH_4 production on

2Cr-$B_{38}N_{38}$ nanocage is 0.34, 0.27, 0.31, 0.24 and 0.22 V. The over-potential of CO_2-RR on 2Cr-C_{76} and 2Cr-$B_{38}N_{38}$ are lower than Fe, Ni and Co single atom as catalysts, Cu, Au, Ag based bimetallic catalysts and Pt and Pd as metal catalysts in previous works. The 2Cr-Si_{76} and 2Cr-$B_{38}N_{38}$ nanocages has higher $\Delta G_{reaction}$ and lower $E_{barrier}$ than 2Cr-C_{76} for CO_2-RR. The over-potential of creation of CH_4 and CH_3OH on 2Cr-Si_{76}, 2Cr-C_{76} and 2Cr-$B_{38}N_{38}$ are lower than HCOOH and HCHO. Finally, the 2Cr-Si_{76}, 2Cr-C_{76} and 2Cr-$B_{38}N_{38}$ are suggested as catalysts for CO_2-RR to create the CO, CH_4, HCOOH, HCHO and CH_3OH with high performance.

Acknowledgment

I thank for my university for computational support.

Ethical approval

All procedures performed in studies involving human participants were in accordance with the ethical standards of the institutional and/or national research committee and with the 1964 Helsinki declaration and its later amendments or comparable ethical standards.

References

1. S. Yousaf, I. Ahmad, A. Ali. Atomically Dispersed Cu Catalysts on Sulfide-Derived Defective Ag Nanowires for Electrochemical CO_2 Reduction, *Mat. Adv*., **5** 7891 (2024).
2. M. S. Hussain, S. Ahmed, DFT Studies on a Metal Oxide@Graphene-Decorated D−π_1–π_2–A Novel Multi-Junction Light-Harvesting System for Efficient Dye-Sensitized Solar Cell Applications, *Nano Mat. Sci.*, **529**, 9001 (2024).
3. A. Faraz, W. Iqbal, S. Gul, Selective electroreduction of CO_2 into CO over Ag and Cu decorated carbon nanoflakes, *Energy Adv.*, **3**, 2367 (2024).
4. F. Chang, Z. Lin, Y. Liu, Metal–organic framework derived micro-/nano-materials: precise synthesis and clean energy applications, *Inorg. Chem. Frontiers*, **11** 5964 (2024).
5. J. Yao, C. Li, K. Sun, Y. Cai, H. Li, W. Ouyang, H. Li, Ndc-scene: Boost monocular 3d semantic scene completion in normalized device coordinates space. *IEEE/CVF Int. Computer Vision* **11**, 9455 (2023).
6. P. Li, J. Abbas, D. Balsalobre-Lorente, Q. Wang, Q. Zhang, S. A. R. Shah, Impact of sectoral mix on environmental sustainability: How is heterogeneity addressed? *Gondwana Res.* **128**, 86 (2024).
7. J. X. Chen, L. Peng, J. Ma, H. P. Ying, Liberation of a pinned spiral wave by a rotating electric pulse. *Euro. phys. Lett.*, **107**, 38001 (2014).
8. X. Sun, S. Zhu, J. Guo, S. Peng, X. Qie, Z. Yu, P. Li, exploring ways to improve China's ecological well-being amidst air pollution challenges using mixed methods. *J. Environ. Management*, **364**, 121457 (2024).
9. M. Wang, W. Xu, H. Xu, H. Mu, J. Mi, Y. Wu, B. Cai, Evaluation of mechanical properties and geological features of highly sandy dolomite: consequences for engineering safety. *Bulletin Eng. Geology Environ*., **84**, 603 (2025).
10. S. Jiang, J. Zhang, K. Diao, X. Liu, Z. Ding, Research Advances in Solvent Extraction of Lithium: The Potential of Ionic Liquids. *Adv. Functional Mat.*, **11**, 2423566 (2025).
11. X. Sun, Z. Meng, X. Zhang, J. Wu, The role of institutional quality in the nexus between green financing and sustainable development. *Res. Int. Business Finance*, **73**, 102531 (2025).
12. M. M. Khotbehsara, M. Zadshir, B. M. Miyandehi, E. Mohseni, S. Rahmannia, S. Fathi, Rheological, mechanical and durability properties of self-compacting mortar containing nano-TiO2 and fly ash. *J. American Sci.*, **10**, 222 (2014).
13. B. Mehdizadeh, K. Vessalas, B. Ben, A. Castel, S. Deilami, H. Asadi, Advances in Characterization of Carbonation Behavior in Slag-Based Concrete Using Nanotomography. *Int. Variability*, **1**, 297 (2022).
14. B. Mehdizadeh Miyandehi, K. Vessalas, A. Castel, M. Mortazavi, Investigation of Carbonation Behaviour in High-Volume GGBFS Concrete for Rigid Road Pavements. *ASCP* **1**, 12 (2023).
15. A. Naseri, B. Maleki, T. Asheghi Mehmandari, A. Tohidi, A. Fahimifar, Investigating the influence of Sample geometric variations on mechanical characterization in rock and concrete. *J. Mining Environ.*, **16**, 1089 (2025).
16. P. Jafari, E. Rasekh, T. Asheghi Mehmandari, M. Mohammadifar, A. Fahimifar, D. Jahed Armaghani, Upper-bound solutions for active face failure in shallow rectangular tunnels in anisotropic and non-homogeneous undrained clays. *Geotech. Geolog. Eng.*, **83**, 1 (2025).
17. T. A. Mehmandari, M. Shokouhian, M. Imani, A. Fahimifar, Experimental and numerical analysis of tunnel primary support using recycled, and hybrid fiber reinforced shotcrete. *In Structures*, **63**, 106282 (2024).
18. Mehmandari, T. A., Shokouhian, M., Imani, M., Tee, K. F., Fahimifar, A. Split Tensile Behavior

of Recycled Steel Fiber-Reinforced Concrete. *ACI Mat. J.*, **122**, 5147 (2025).
19. T. A. Mehmandari, M. Shokouhian, M. Z. Josheghan, S. A. Mirjafari, A. Fahimifar, D. J. Armaghani, K. F. Tee, Flexural properties of fiber-reinforced concrete using hybrid recycled steel fibers and manufactured steel fibers. *J. Building Eng.*, **98**, 111069 (2024).
20. T. A. Mehmandari, D. Mohammadi, M. Ahmadi, M. Mohammadifar, Fracture mechanism and ductility performances of fiber reinforced shotcrete under flexural loading insights from digital image correlation (DIC). *Insight Civil Eng.*, **7**, 611 (2024).
21. M. Ershadi, M. Javanbakht, D. Brandell, S. A. Mozaffari, A. M. Aghdam, Facile synthesis of amino-functionalized mesoporous Fe3O4/rGO 3D nanocomposite by diamine compounds as Li-ion battery anodes. *Appl. Sur. Sci.*, **601**, 154120 (2022).
22. A. Molaei Aghdam, S. Habibzadeh, M. Javanbakht, M. Ershadi, M. R. Ganjali, High interspace-layer manganese selenide nanorods as a high-performance cathode for aqueous zinc-ion batteries. *ACS Appl. Energy Mat.*, **6**, 3225 (2023).
23. A. Molaei Aghdam, N. Mikaeili Chahartagh, E. Delfani, High-Efficient Capacitive Deionization Using Amine-Functionalized ZIF-67@2D MXene: Toward Ultrahigh Desalination Performance. *Adv. Mat. Techn.*, **8**, 2300628 (2023).
24. A. M. Aghdam, N. M. Chahartagh, S. Namvar, M. Ershadi, F. B. Ajdari, E. Delfani, Improving the performance of a SnS 2 cathode with interspace layer engineering using a Na+ insertion/extraction method for aqueous zinc ion batteries. *J. Mat. Chem. A*, **12**, 1047 (2024).
25. F. B. Ajdari, F. Abbasi, A. M. Aghdam, F. G. C. Khaneh, A. G. Arjenaki, V. Farzaneh, S. Ramakrishna, Innovative self-repairing binders tackling degradation and de-lithiation challenges: Structure, mechanism, high energy and durability. *Mat. Sci. Eng. Reports*, **160**, 100830 (2024).
26. F. B. Ajdari, P. Asghari, A. Molaei Aghdam, F. Abbasi, R. P. Rao, A. Abbasi, M. N. Chahartagh, Silicon Solid State Battery: The Solid-State Compatibility, Particle Size, and Carbon Compositing for High Energy Density. *Adv. Functional Mat.*, **34**, 2314822 (2024).
27. N. M. Chahartagh, A. M. Aghdam, S. Namvar, M. Jafari, Enhancing the performance and cyclability of MoS 2 cathodes with interspace layer engineering using polypyrrole. *J. Mat. Chem. A*, **12**, 10875 (2024).
28. K. Hooshyari, A. M. Aghdam, M. B. Karimi, P. Salarizadeh, M. Moradi, S. Rahmani, M. Tohidian, Lithium-Ion Batteries: Fundamental Principles, Recent Trends, Nanostructured Electrode Materials, Electrolytes, Promises, Key Scientific and Technological Challenges, and Future Directions. *Nanostruct. Mat. Energy Storage*, **1**, 31 (2024).
29. M. N. Chahartagh, A. Molaei Aghdam, S. Namvar, F. Boorboor Ajdari, M. Ershadi, M. Jafari, Conductive Polymer Designed of Binder-Free Polypyrrole-MnO2/Ti3C2 for Oxidative Stable Aqueous Zinc-Ion Batteries. *ACS Appl. Energy Mat.* **1**, 12 (2025).
30. A. M. Aghdam, K. Valizadeh, A. Bateni, N. Sojoodi, M. S. Jahanian, A. Kumar, J. Giao, Potential of Cu-CNT (8, 0), V-C52, and Zn-SiNT (7, 0) catalysts for CO2 reduction to CH3OH. *J. Molec. Liq.*, **360**, 119464 (2022).
31. F. Abbasi, F. Boorboor Ajdari, M. Mansournia, P. Asghari, A. Molaei Aghdam, Toward high energy and durable anodes: critical review on Li4Ti5O12–MXene composites. *Carbon Lett.*, **1**, 23 (2025).
32. Y. Ru, M. Gruninger, Y. Dou, Robust self-supervised symmetric nonnegative matrix factorization to the graph clustering. *Sci. Reports*, **15**, 7350 (2025).
33. Y. Huo, S. Gang, C. Guan, Fcihmrt: *Feature cross-layer interaction hybrid method based on Res2Net and transformer for remote sensing scene classification, Electronics*, **12**, 4362 (2023).
34. J. Singh, R. Abraham, Magnetic Catalyst CdFe2O4: Direct Conversion of Thiols into Antibacterial Sulfonamides. *Biol. Mol. Chem.*, **2**, 13 (2024).